Electronic Supporting Information

Novel high-entropy layered double hydroxide microspheres as effective and durable electrocatalyst for oxygen evolution

Shun Li[a], Likai Tong[a], Zhijian Peng[b,*], Bo Zhang[a] and Xiuli Fu[a,*]

[a] *School of Integrated Circuits, Beijing University of Posts and Telecommunications, Beijing 100876, P. R. China*

[b] *School of Science, China University of Geosciences, Beijing 100083, P. R. China*

Corresponding authors

* *Telephone: 86-10-62282452. Fax: 86-10-62282054*

E-mail: xiulifu@bupt.edu.cn (X. Fu) and pengzhijian@cugb.edu.cn

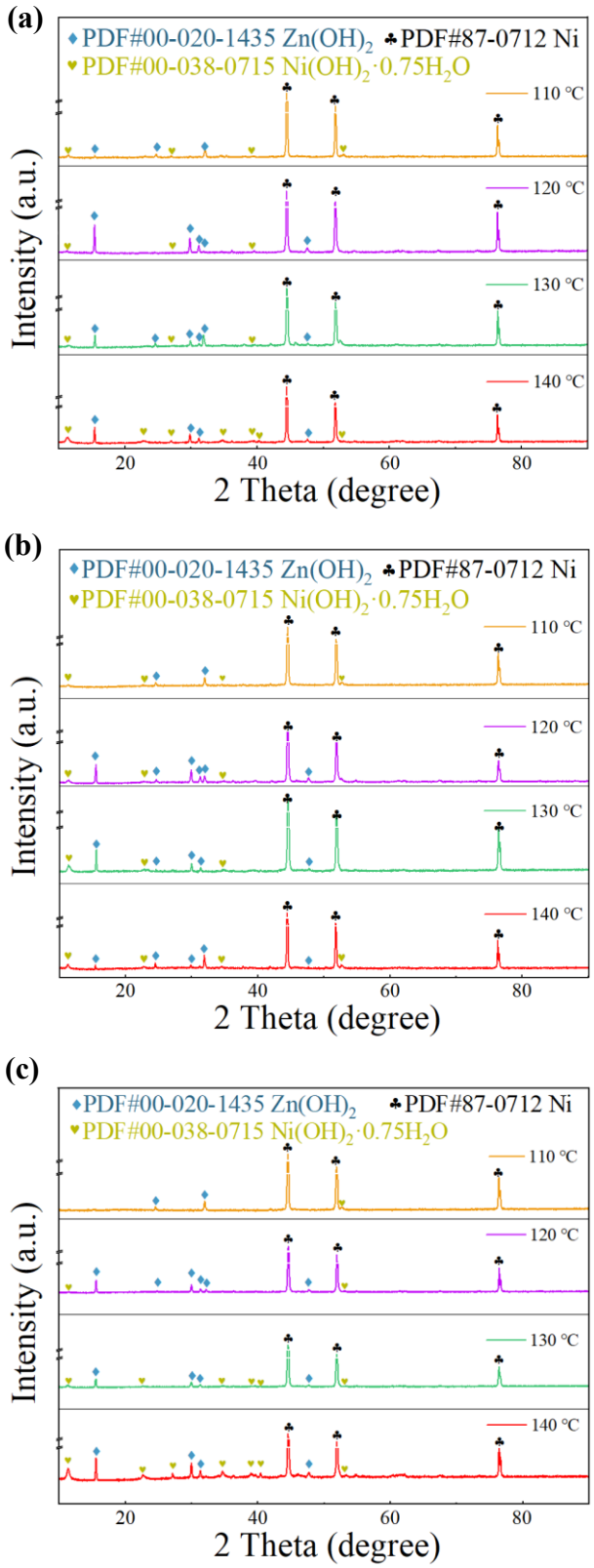

Fig. S1 X-ray diffraction patterns of (a) HELDH-M/NF, (b) HELDH-C/NF and (c) HELDH-MC/NF prepared at 110-140 ºC.

As is seen in Fig. S1, the three strong peaks at 44.5°, 51.8° and 76.4° in all the XRD patterns are assigned to the Ni foam substrate (PDF#87-0712) in the synthesized HELDH samples. Moreover, the diffraction peaks of all the three HELDH samples prepared at 120 ºC could be well indexed to those of $Zn(OH)_2$ phase, implying that 120 ºC is the optimal synthesis temperature. This is because the formation energy of a high-entropy structure is generally high, a temperature lower than 120 °C is not high enough for a variety of elements to be integrated into the lattice to form high-entropy hydroxides. However, as the synthesis temperature increases, the diffraction peaks of $Ni(OH)_2 \cdot 0.75H_2O$ become more and more obviously, because a higher temperature allows more Ni from the Ni foam substrate to continue reacting and forming hydroxide $Ni(OH)_2$.

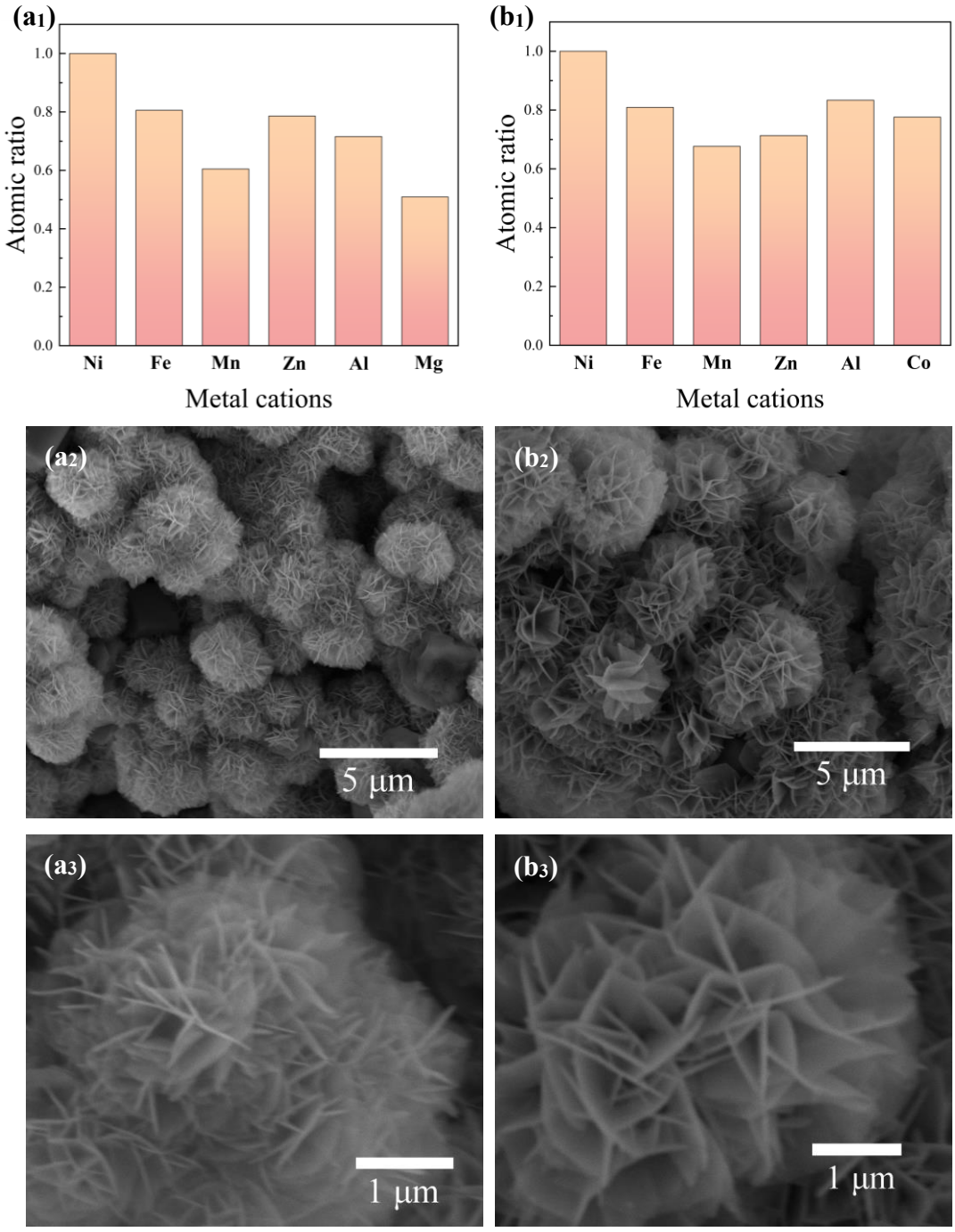

Fig. S2 Atomic ratios (a_1, b_1) measured by ICP technique, low-magnification SEM images (a_2, b_2) and high-magnification SEM images (a_3, b_3) of HELDH-M (a) and HELDH-C (b), respectively.

As shown in Fig. S2(a_1, b_1), the theoretical ratio of the constituent elements (assuming equal atomic proportions) was nearly achieved in the as-synthesized samples. Specifically, it is noted that for the two HELDH samples, the content of Ni is higher than those of the other metal elements,

probably because all the HELDH samples are grown on the Ni foam substrate, which can also provide a small amount of Ni source during the synthesis process. Moreover, from the low-magnification SEM images as shown in Fig. S2(a_2, b_2), it is seen that both six-membered HELDH samples are composed of lots of regular nanoflower-like microspheres. From the high-magnification SEM images as shown in Fig. S2(a_3, b_3), it is observed that each microsphere indeed consists of a large number of nanosheets, revealing that the two six-element high entropy structures are successfully synthesized.

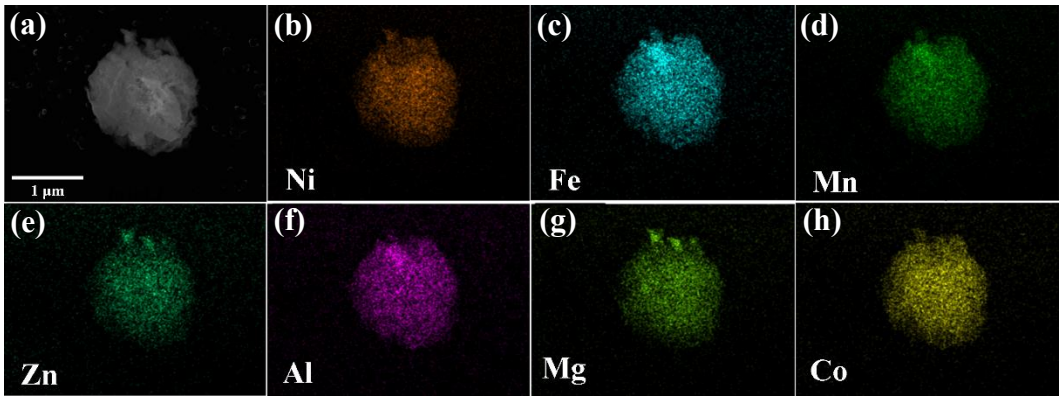

Fig. S3 SEM-EDX mapping scanning area (a) and (b-h) the recorded mapping images of Ni, Fe, Mn, Zn, Al, Mg, and Co in HELDH-MC sample.

As is seen in **Fig. S3**, the energy dispersive X-ray (EDX) mapping of the HELDH-MC micorspheres confirms that the corresponding seven metal elements are uniformly distributed within the nanosheets, which aligns well with the data of ICP-OES. To some extent, this highly elements-dispersive structure guarantees a large configurational entropy of the HELDHs.

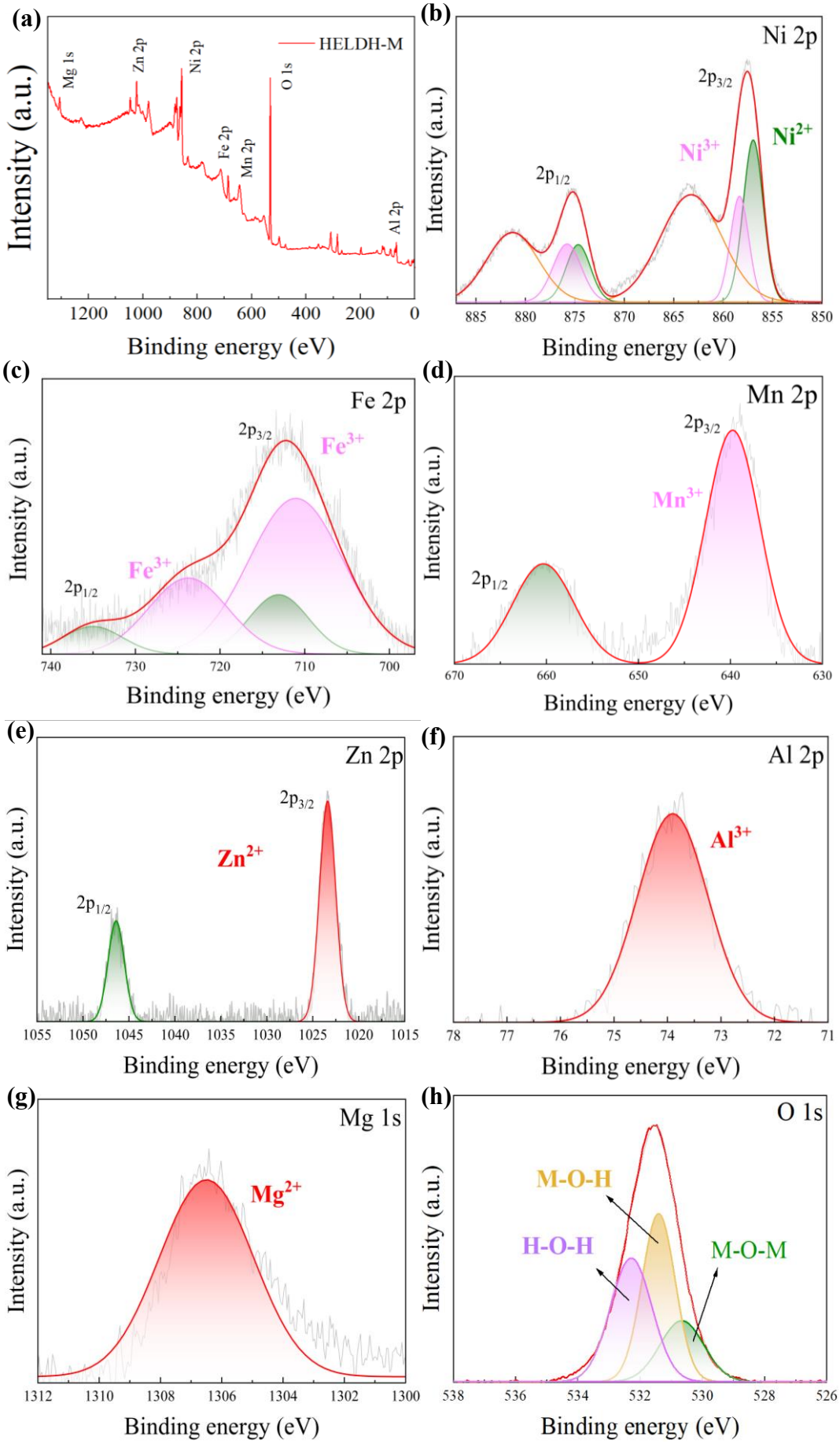
(a)
HELDH-M
Mg 1s
Zn 2p
Ni 2p
Fe 2p
Mn 2p
O 1s
Al 2p
Intensity (a.u.)
Binding energy (eV)
(b)
Ni 2p
2p3/2
2p1/2
Ni3+
Ni2+
(c)
Fe 2p
Fe3+
(d)
Mn 2p
Mn3+
(e)
Zn 2p
Zn2+
(f)
Al 2p
Al3+
(g)
Mg 1s
Mg2+
(h)
O 1s
M-O-H
H-O-H
M-O-M

Fig. S4 XPS data of HELDH-M sample. (a) XPS survey spectrum and the high-resolution spectra of (b) Ni 2p, (c) Fe 2p, (d) Mn 2p, (e) Zn 2p, (f) Al 2p, (g) Mg 1s and (h) O 1s.

As seen in Fig. S4a, the XPS survey spectrum of the optimal HELDH-M confirms the coexistence of Ni, Fe, Mn, Zn, Al, Mg, and O in the sample. In Fig. S4b, the peak fitting of the high-resolution Ni 2p spectrum reveals that the peaks centered at 2p3/2 (856.9 eV) and 2p1/2 (874.6 eV) with two shake-up satellites correspond to the presence of Ni^{2+} species, while the peaks at 2p3/2 (858.3 eV) and 2p1/2 (875.8 eV) with two shake-up satellites are attributed to the presence of Ni^{3+} species. The high-resolution Fe 2p spectrum (Fig. S4c) exhibits two broad peaks that can be fitted into four peaks. Among them, Fe $2p_{3/2}$ and Fe $2p_{1/2}$ are located at around 710.9 and 723.8 eV, respectively, indicating that the iron atom in HELDH-M is present as Fe^{3+}. For the high-resolution spectrum of Mn 2p (Fig. S4d), the two peaks centered at 639.6 and 660.4 eV can be attributed to Mn $2p_{3/2}$ and Mn$2p_{1/2}$ of Mn^{3+} in the sample, respectively. Especially, the spectrum of Mn 2p shows peaks similar to those of MnOOH and Mn_2O_3, indicating the presence of Mn^{3+} in the product. As seen in Fig. S4e for the high-resolution spectrum of Zn 2p, there are two sharp peaks located at 1023.1 (Zn $2p_{3/2}$) and 1047.2 eV (Zn $2p_{1/2}$), respectively, where the Zn $2p_{3/2}$ spectrum can be attributed to Zn^{2+}. The high-resolution spectrum of Al 2p (Fig. S4f) shows a strong, sharp peak at 73.9 eV, which can be indexed to Al 2p3/2 of Al^{3+} in the sample. For the high-resolution XPS spectrum of Mg 1s (Fig. S4g), the only strong peak centered at 1306.5 eV is attributed to the bivalent state of Mg^{2+}. In addition, the broad peak in the high-resolution spectrum of O 1s (Fig. S4h) results from the combination of two individual peaks at 531.4 and 530.65 eV, which correspond to the appearance of O-containing groups with M-O-H and M-O-M structures, respectively.

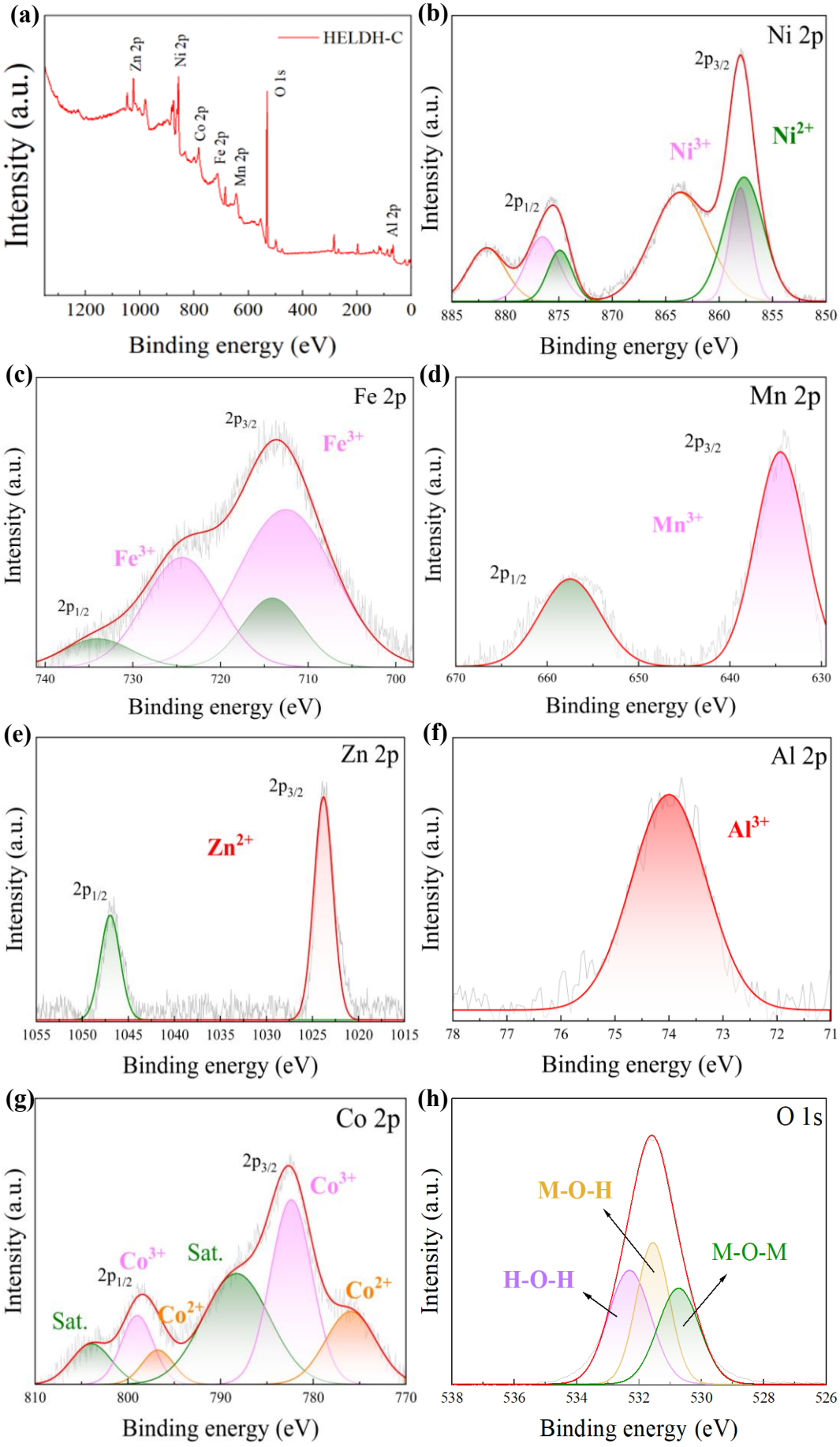
(a)
HELDH-C
Zn 2p
Ni 2p
Co 2p
Fe 2p
Mn 2p
O 1s
Al 2p
Intensity (a.u.)
Binding energy (eV)
(b)
Ni 2p
2p3/2
2p1/2
Ni3+
Ni2+
(c)
Fe 2p
Fe3+
Fe3+
2p3/2
2p1/2
(d)
Mn 2p
2p3/2
Mn3+
2p1/2
(e)
Zn 2p
2p3/2
Zn2+
2p1/2
(f)
Al 2p
Al3+
(g)
Co 2p
2p3/2
Co3+
Co3+
Sat.
2p1/2
Co2+
Sat.
Co2+
(h)
O 1s
M-O-H
M-O-M
H-O-H

Fig. S5 XPS data of HELDH-C sample. (a) XPS survey spectrum and the high-resolution spectra of (b) Ni 2p, (c) Fe 2p, (d) Mn 2p, (e) Zn 2p, (f) Al 2p, (g) Co 2p and (h) O 1s.

As shown in Fig. S5a, the XPS survey spectrum of the optimal HELDH-C indicates the coexistence of Ni, Fe, Mn, Zn, Al, Co, and O in the sample. In Fig. S5b, the peak fitting of high-resolution Ni 2p spectrum reveals that the peaks centered at 2p3/2 (857.6 eV) and 2p1/2 (874.9 eV) with two shakeup satellites are attributed to the presence of Ni^{2+} species, while the peaks at 2p3/2 (858 eV) and 2p1/2 (876.5 eV) with two shakeup satellites are due to the presence of Ni^{3+} species. The high-resolution Fe 2p spectrum (Fig. S5c) presents two broad peaks that can be deconvoluted into four peaks. Among them, Fe $2p_{3/2}$ and Fe $2p_{1/2}$ are located at around 712.8 and 724.9 eV, respectively, indicating that the iron atom in HELDH-C is present as Fe^{3+}. For the high-resolution spectrum of Mn 2p (Fig. S5d), the two peaks centered at 634.5 and 657.6 eV can be attributed to Mn $2p_{3/2}$ and Mn $2p_{1/2}$ of Mn^{3+} in the sample. Especially, the spectrum of Mn 2p shows peaks similar to those of MnOOH and Mn_2O_3, indicating the presence of Mn^{3+} in the product. As seen in Fig. S5e for the high-resolution spectrum of Zn 2p, there are two sharp peaks located at 1023.2 (Zn $2p_{3/2}$) and 1047.8 eV (Zn $2p_{1/2}$), respectively, where the Zn $2p_{3/2}$ spectrum can be attributed to Zn^{2+}. For the high-resolution spectrum of Al 2p (Fig. S5f), the strong, sharp peak at 74 eV is indexed to Al 2p3/2 of Al^{3+} in the sample. In Fig. S5g, two peak components can be fitted with the Co$2p_{3/2}$ and Co $2p_{1/2}$, indicating the existence of the Co^{2+} and Co^{3+} in the sample. In addition, the broad peak in the high-resolution spectrum of O 1s (Fig. S5h) is due to the combination of two individual peaks at 531.7 and 530.7 eV, which are correlated to the appearance of O-containing groups with M−O−H and M−O−M structures, respectively.

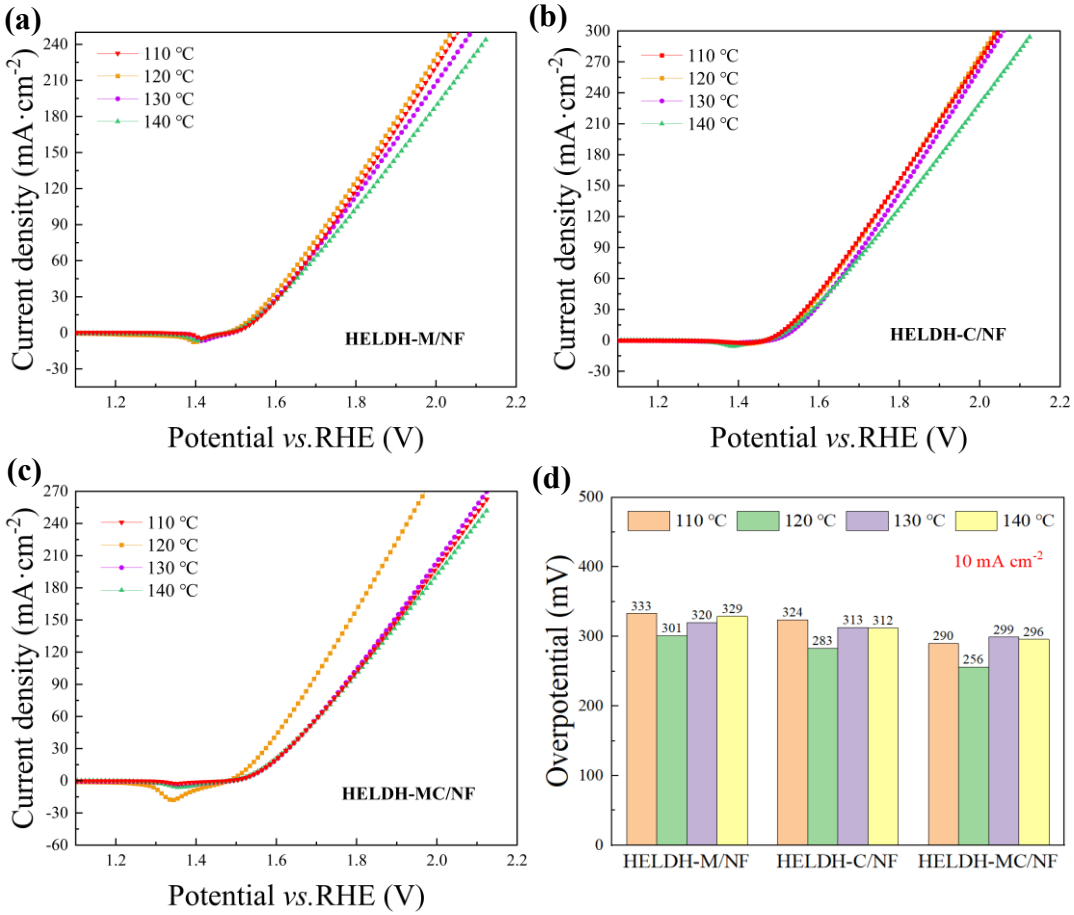

Fig. S6 Polarization curves of (a) HELDH-M/NF, (b) HELDH-C/NF and (c) HELDE-MC/NF prepared at different temperatures. (d) The required overpotentials at 10 mA cm^{-2}.

The oxygen evolution performances of HELHD-M/NF, HELHD-C/NF, and HELDH-MC/NF synthesized at different temperatures are shown in Fig. S6(a–c). The comparison on the required overpotentials is exhibited directly in Fig. S6d. It can be seen that regardless of the type of HELDH, the samples synthesized at 120 ºC show the best oxygen evolution performance, which is consistent with the XRD results. It can also be observed that the performance of HELDH-MC/NF is better than those of the other two hexahydroxy HELDH samples, which may be due to the synergistic effect between the elements.

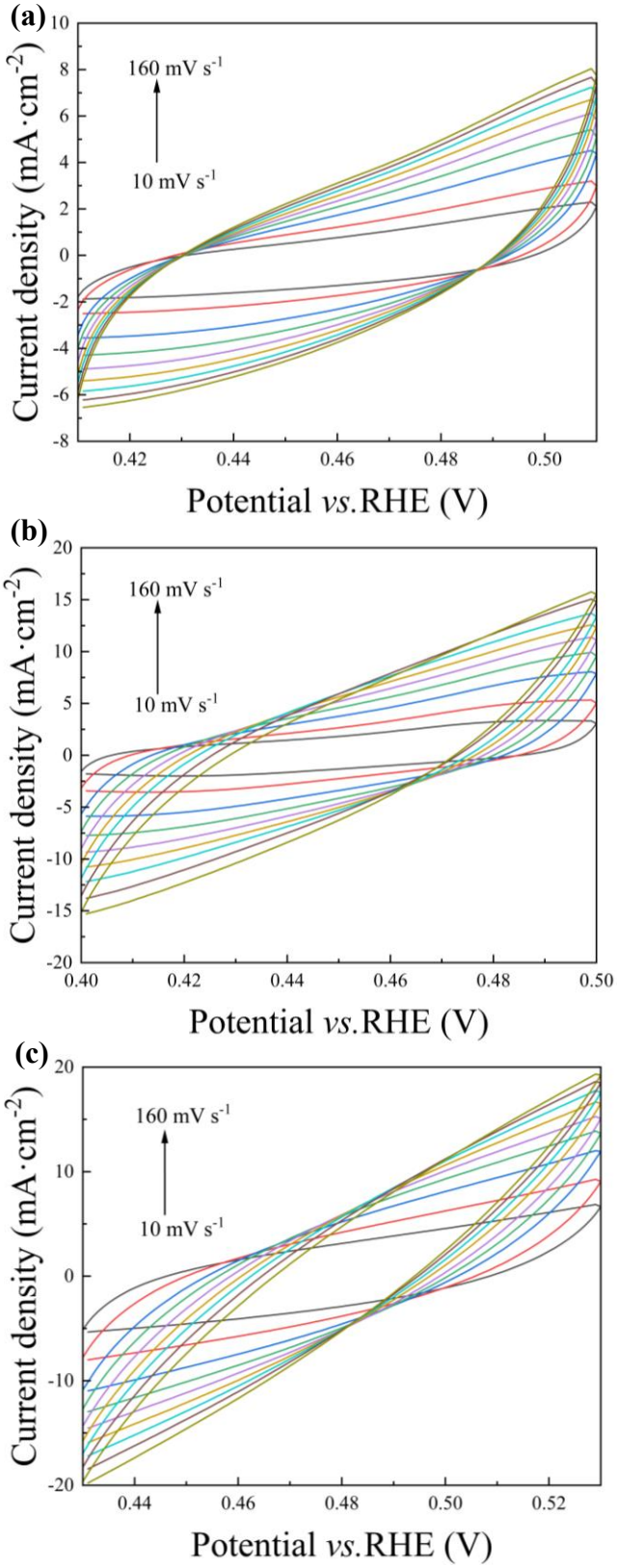

Fig. S7 Cyclic voltammograms of (a) HELDH-M/NF, (b) HELDH-C/NF and (c) HELDH-MC/NF.

In order to obtain ECSA, CV tests were conducted on HELDHs at 10–160 mV s^{-1}.

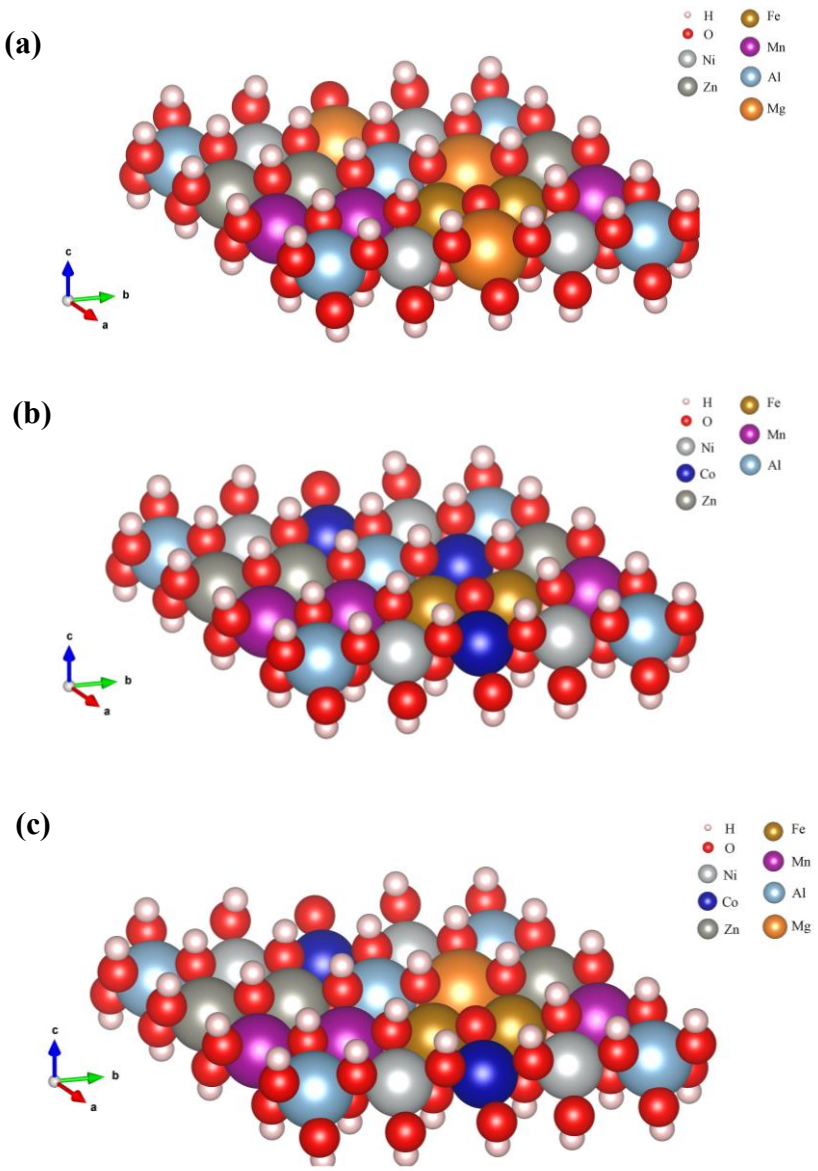

Fig. S8 The optimized structures of (a) HELDH-M, (b) HELDH-C, and (c) HELDH-MC.

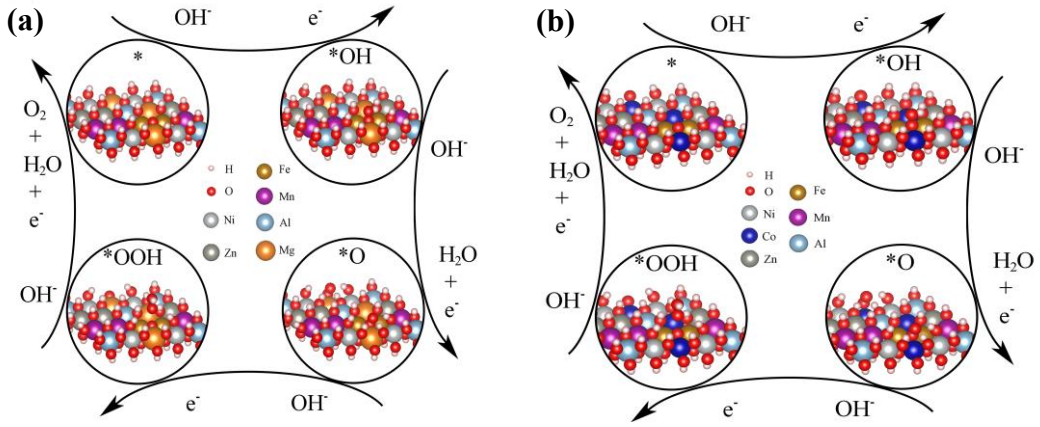

Fig. S9 OER processes on the surface of (a) HELDH-M, and (b) HELDH-C catalysts.

Table S1 DFT calculated energy, zero-point energy, entropy, and Gibbs free energy of the gas phase molecules considered in this work.

Molecule	E/eV	ZPE/eV	-TS/eV	G/eV
H_2O	-14.22	0.58	-0.67	-14.31
H_2	-6.77	0.27	-0.40	-6.90

Table S2 DFT calculated zero-point energy of the intermediates onto different models in this work.

DFT models	$\Delta E_{ZPE}(H_2O*)$	$\Delta E_{ZPE}(OH*)$	$\Delta E_{ZPE}(O*)$	$\Delta E_{ZPE}(OOH*)$
HELDH-C	0.5944	0.3485	0.0668	0.3689
HELDH-M	0.5810	0.3602	0.0695	0.3862
HELDH-MC	0.7939	0.3472	0.0662	0.3625

Table S3 The changes of Gibbs free energy of H/O containing intermediates and calculated theoretical overpotentials for OER at 0 V.

DFT models	$\Delta G_{\mathrm{OH}*}$ (eV)	$\Delta G_{\mathrm{O}*}$ (eV)	$\Delta G_{\mathrm{OOH}*}$ (eV)	ΔG_1 (eV)	ΔG_2 (eV)	ΔG_3 (eV)	ΔG_4 (eV)	$\eta_{\mathrm{t,OER}}$ (V)
HELDH-C	3.03	2.94	4.48	3.03	-0.09	1.54	0.48	1.80
HELDH-M	3.32	2.88	4.50	3.32	-0.45	1.63	0.46	2.09
HELDH-MC	1.80	2.25	3.79	1.80	0.45	1.54	1.17	0.57

Table S4 The changes of Gibbs free energy of H/O containing intermediates for OER at 1.23 V.

DFT models	$\Delta G_{\mathrm{OH}*}$ (eV)	$\Delta G_{\mathrm{O}*}$ (eV)	$\Delta G_{\mathrm{OOH}*}$ (eV)	ΔG_1 (eV)	ΔG_2 (eV)	ΔG_3 (eV)	ΔG_4 (eV)
HELDH-C	1.80	0.48	0.79	1.80	-1.32	0.31	-0.75
HELDH-M	2.09	0.42	0.81	2.09	-1.68	0.40	-0.77
HELDH-MC	0.57	-0.21	0.1	0.57	-0.78	0.31	-0.06